ACS Photonics

Article

pubs.acs.org/journal/apchd5

Competition between Förster Resonance Energy Transfer and Donor Photodynamics in Plasmonic Dimer Nanoantennas

Sébastien Bidault,[†] Alexis Devilez,[‡] Petru Ghenuche,[‡,§] Brian Stout,[‡] Nicolas Bonod,[‡] and Jérôme Wenger*[,‡]

[†]ESPCI Paris, PSL Research University, CNRS, INSERM, Institut Langevin, 75005 Paris, France

[‡]CNRS, Aix-Marseille Université, Centrale Marseille, Institut Fresnel, UMR 7249, 13013 Marseille, France

Supporting Information

ABSTRACT: Plasmonic optical antennas enhance and control the emission of quantum sources in the far-field. Interestingly, the antenna concept can also be applied to enhance the electric field produced by a quantum emitter in the near-field and increase the rate of Förster resonance energy transfer (FRET) between two nearby donor and acceptor dipole emitters. However, plasmonic antennas also influence numerous other photophysical processes such as the donor excitation intensity and decay dynamics and the acceptor emission yield, which compete with the observation of FRET. Understanding the balance between FRET and these processes and monitoring FRET under intense resonant optical confinement in plasmonic nanoantennas have remained challenging open questions. Here, we use DNA-driven self-assembly to accurately produce 40 and 60 nm gold nanoparticle dimer antennas containing a single FRET pair located in the center of a 14 nm gap. The spontaneous donor decay rate constants are increased by 2 orders of magnitude, creating high local densities of optical states (LDOS) to explore the link between LDOS and FRET. The antennas induce a 5-fold increase of Förster energy transfer rate constants associated with reduced transfer efficiencies, in good agreement with numerical simulations. The strong antenna−emitter interaction leads to the surprising association of an enhanced acceptor emission with a weak transfer efficiency. Our measurements exemplify the competition between radiative and nonradiative processes in complex nanophotonic systems and highlight geometrical parameters and design rules to optimize nanoantennas for nonradiative energy harvesting.

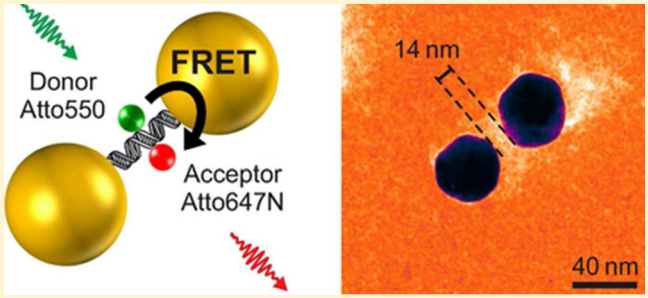

KEYWORDS: *plasmonics, nanoantenna, FRET, LDOS, fluorescence enhancement, gold nanoparticle, DNA self-assembly*

Förster resonance energy transfer (FRET) describes the nonradiative transfer of electronic excitation energy from an excited donor to a ground-state acceptor molecule occurring on nanometer scale distances.[1,2] FRET plays a key role in photosynthesis,[3] organic photovoltaics,[4] lighting sources,[5] and biosensing.[6] In single-molecule fluorescence applications, FRET is widely used to measure the distance between two fluorescent sources at the nanometer scale,[7,8] enabling the study of molecular conformations[9] and interaction dynamics.[10]

It is now well established that the fluorescence emission from single-quantum emitters can be controlled by the photonic environment via the local density of optical states (LDOS).[11−14] An enhanced LDOS in optical resonators leads to a faster decay from the emitter's electronic excited state, as a result of the interaction of the emitter with its own secondary field backscattered by the local environment.[11] At the level of individual emitters, this concept has allowed the enhancement of fluorescence decay rates and intensities from single molecules in top-down fabricated[15−17] and self-assembled[18−23] plasmonic nanoantennas.

However, applying the nanophotonic concepts to the donor−acceptor FRET is more complex than a simple two-emitter extension. A broadband optical resonator increasing the electric field produced by a donor molecule at the position of an acceptor should also enhance the Förster energy transfer rate.[11] On the other hand, FRET near an optical nanoantenna competes with other decay processes from the donor excited state (radiative emission and ohmic losses to the metal), so that a strongly enhanced LDOS can lead to reduced transfer efficiencies. Finally, ohmic losses in the nanoantenna can reduce the acceptor emission, increasing the challenge to measure the FRET rate constant and efficiency. The broad range of conditions in which the photonic environment could influence nonradiative transfer processes has been highlighted by several theoretical studies.[24−30] Experimentally, ensemble FRET measurements in microcavities[31−33] and arrays of nanoparticles[34,35] suggested a dependence of the transfer rate constant on the LDOS due to an inhomogeneous photonic environment. This trend was confirmed at the single FRET pair level by experiments on metal nanoapertures[36,37] and an

Received: February 29, 2016
Published: April 12, 2016

DOI: 10.1021/acsphotonics.6b00148
ACS Photonics 2016, 3, 895−903

aluminum optical gap antenna.[38] However, reports on mirrors,[39−41] microresonators,[42,43] and dielectric nanoparticles[44,45] observed negligible changes of the FRET rate constant.

The LDOS enhancement is an indicative figure of merit to compare the different nanophotonic architectures and reveal the overall acceleration of the donor decay dynamics.[11] Nonresonant structures feature modest LDOS enhancements, with a maximum of 1.5× with planar mirrors,[39] 2.3× with microcavities,[31] or 2.9× with nanoapertures.[36,37] Resonant aluminum gap antennas provide higher values up to 10-fold, leading to a more significant 5-fold enhancement in the FRET rate constant between donor and acceptor dyes separated by 10 nm.[38] However, these examples remain modest as compared to the capabilities of optimized plasmonic nanoantennas, where excited-state decay rates can be reproducibly enhanced by more than 2 orders of magnitude.[18,19,21] Earlier work on FRET in gold nanoparticle dimer antennas observed an acceleration of the Förster rate constant,[27] but FRET pairs nonspecifically bound all around the nanoparticles dominated the optical response and challenged the analysis of FRET pairs in the gap of the antenna. Therefore, the influence of large, >100×, LDOS variations on the FRET process remains an open question, which is essential to determine the limits of the FRET tunability using nanophotonics.

In this work, we investigate FRET between single donor and acceptor dyes inside the nanogap of a resonant plasmonic gold dimer antenna featuring LDOS enhancements up to 150×. DNA-driven self-assembly and electrophoretic purification are used to produce suspensions of 40 and 60 nm gold nanoparticle dimers containing a single FRET pair in the center of a 14 nm gap (Figure 1a). The spontaneous donor decay rate constants are increased by more than 100-fold, allowing the exploration of FRET in intense LDOS conditions. Furthermore, changing the particle size tunes the relative strength of ohmic losses in the antenna with respect to far-field radiation. In contrast to our previous work on lithographied aluminum nanoantennas where the FRET constructs were randomly diffusing around the antenna hot spots,[38] the present study uses DNA-driven self-assembly to accurately position the fluorescent donor and acceptor emitters inside the nanogap. Importantly to assess the validity of our conclusions, all the experiments are performed at the single FRET pair level by recording simultaneously the donor and the acceptor emission photodynamics. This provides two independent measurements to characterize FRET by monitoring either the donor lifetime reduction in the presence of the acceptor or the relative intensities of the donor and acceptor fluorescence. We demonstrate a 5-fold increase of Förster energy transfer rate constants associated with reduced transfer efficiencies in plasmonic nanoantennas, in good agreement with numerical simulations. Our results also point out perplexing configurations where the highest acceptor fluorescence signal is observed with the lowest transfer efficiency, while the weakest acceptor emission is associated with the fastest transfer rate. This study forms a focal point in the investigation of FRET in complex nanophotonic environments and highlights important parameters to control nonradiative energy transfer processes in broadband optical resonators.

RESULTS

Purified suspensions of gold nanoparticle dimers, linked preferentially by a single DNA double strand (Figure 1a), are prepared using electrophoretic purification (Supporting Information Figure S1).[19,46−48] We consider two sizes for the gold nanoparticles, using either 40 or 60 nm particles. For both sizes, the interparticle gap distance is set to 14 nm by the 30-base-pair length of the DNA double strand and the trithiolated linking moieties,[48] which are stretched by repulsive electrostatic interactions,[46,49] leading to a ±2 nm standard deviation of interparticle distances as estimated in cryoelectron microscopy.[48,49] Figure 1b shows a high-resolution cryoelectron microscopy image of a 40 nm nanoparticle dimer (see Figure S2 for complementary images with 60 nm particles). A single Atto550 fluorescent donor molecule (quantum yield 80%) and a single Atto647N fluorescent acceptor molecule (quantum yield 65%) are inserted in the middle of the DNA sequence. Therefore, after DNA hybridization, the donor and acceptor molecules are located in the middle of the 14 nm gap on opposite sides of the DNA double helix (Figure 1a). The estimated donor−acceptor separation is 4 ± 1 nm, taking into account the molecular linkers between the conjugated DNA bases and the synthetic dyes.

Dark-field microscopy images (Figure 1c) and scattering spectra (Figure 1d and Supporting Information Figure S3) indicate spectral resonances characteristic of dimer gap antennas.[46] The central resonance wavelengths are at 560 nm for 40 nm dimers and at 585 nm for 60 nm dimers, in good agreement with numerical simulations based on Mie theory.[48]

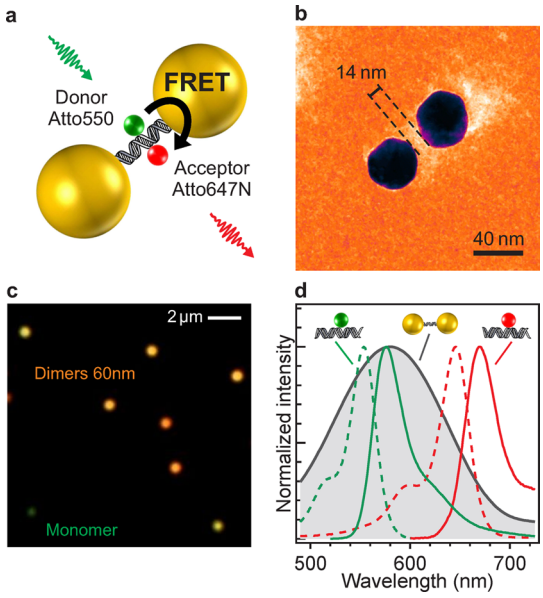

Figure 1. Single donor−acceptor FRET pair in a DNA-templated plasmonic dimer nanoantenna. (a) Sketch of the structure. The donor and acceptor fluorescent dyes are labeled in the middle of the complementary 30-base-long DNA sequences linking the gold nanoparticles. Both dyes stand on opposite sides of the DNA double helix and are axially located in the center of the 14 nm gap between the gold nanoparticles. The donor−acceptor distance is estimated around 4 nm. (b) Cryogenic electron microscopy image of a dimer nanoantenna made of two DNA-templated 40 nm gold nanoparticles separated by a 14 nm gap. (c) Dark-field microscopy image of 60 nm gold nanoparticle dimers on a glass substrate. A single 60 nm gold nanoparticle is also present in the bottom left of the image for direct comparison. (d) Scattering spectrum of the 60 nm dimer nanoantenna (filled gray curve) overlaid on the Atto550 donor and the Atto647N acceptor spectra (green and red curves, respectively, dashed lines for absorption spectra, solid lines for emission spectra).

DOI: 10.1021/acsphotonics.6b00148
ACS Photonics 2016, 3, 895−903

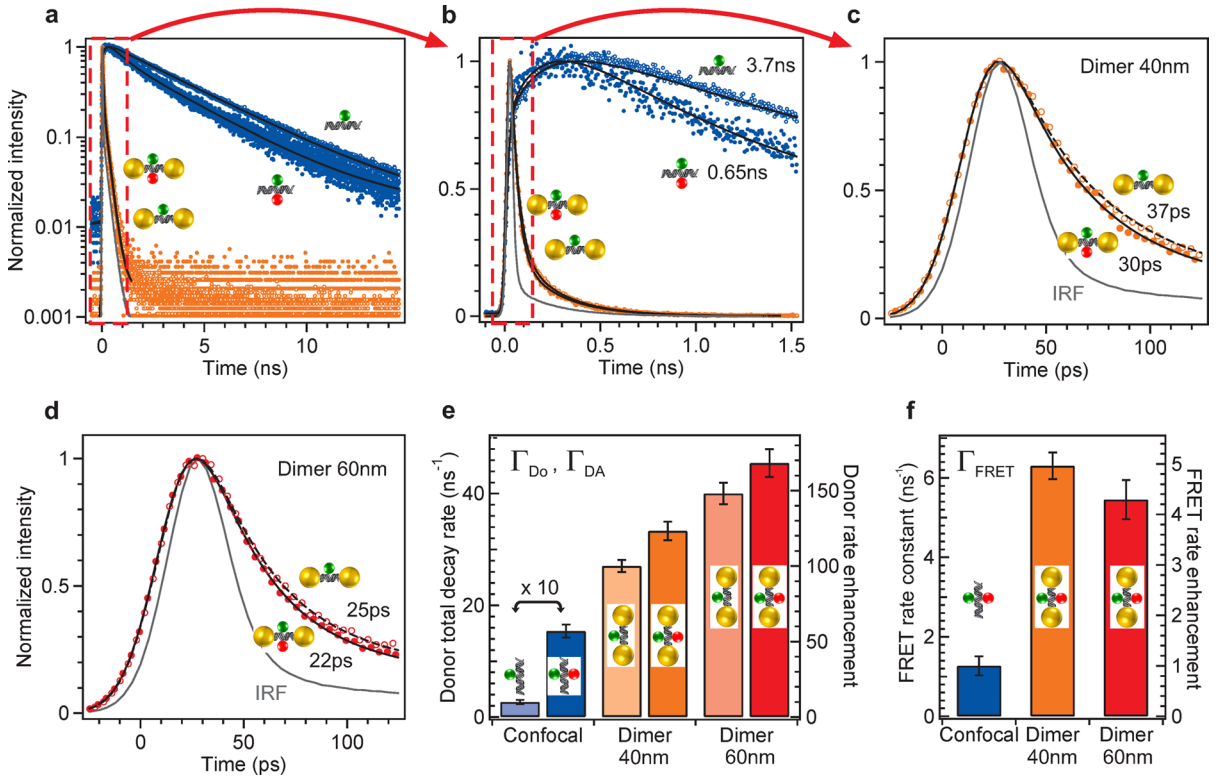

Figure 2. Donor decay acceleration in dimer nanoantennas. (a–c) Normalized donor fluorescence decay traces in the absence (empty markers) and presence (filled markers) of the acceptor dye. The confocal DNA reference without gold nanoparticles is shown in blue traces; the dimer with 40 nm gold nanoparticles corresponds to orange traces. Black lines are numerical fits convoluted by the instrument response function (IRF). The labels refer to the donor fluorescence lifetime (values detailed in Supporting Information Table S1). (d) Same as (c) for dimers of 60 nm nanoparticles to further accelerate the decay. (e) Donor decay rate constant in the absence and presence of the acceptor (respectively Γ_{Do} and Γ_{DA}) for the dimers and the confocal reference (multiplied by 10 for visualization). The rate enhancement (right scale) is defined as compared to the isolated donor decay rate constant in the confocal DNA reference. The error bars are deduced from the uncertainty in the numerical fit of the TCSPC data. (f) FRET rate constant $\Gamma_{FRET} = \Gamma_{DA} - \Gamma_{Do}$ for the different samples. The rate enhancement (right scale) is computed with respect to the confocal DNA reference.

For both diameters, the broad antenna resonance peak significantly overlaps with the donor emission spectrum.

To investigate the energy transfer between dyes within the dimer gap antennas, we combine several time-resolved fluorescence techniques to characterize the fluorescence emission from picoseconds to several seconds.[36−38] Time-correlated single photon counting (TCSPC) quantifies the fluorescence lifetime and decay rate constants, while photon burst analysis records the FRET efficiency histograms, and fluorescence correlation spectroscopy (FCS) quantifies the diffusion properties and the average number of antennas in the detection volume. The implementation of the different techniques and the experimental setup are described in the Methods section. Throughout this study, the dimer antennas are diluted to 100 pM concentration to ensure observing individual dimer antennas as they diffuse across the confocal observation volume. The FCS analysis confirms that less than one antenna is present on average in the confocal volume (Supporting Information Figures S4–S6).

Comparing the time-correlated decay traces with and without the dimer antenna indicates striking reductions of the fluorescence lifetimes for the donor dye (Figure 2a–d and Supporting Information Figure S7). The fluorescence lifetime of the isolated Atto550 donor is reduced from 3.7 ns for the reference without antenna to 37 ± 3 ps with the 40 nm dimer and 25 ± 3 ps with the 60 nm dimer antenna. These extremely short luminescence lifetimes correspond to an acceleration of the decay rate constant Γ_{Do} (inverse of fluorescence lifetime) by 100× for the 40 nm dimer and 150× for the 60 nm dimer (Figure 2e). This high LDOS enhancement is achieved due to the unique combination of (i) narrow gap sizes and (ii) excellent spectral overlap between the antenna plasmonic resonance and the fluorescence emission (Figure 1d). The experimental results also stand in good agreement with numerical simulations based on Mie theory (see Supporting Information Figures S8–S10).

Self-assembled gold particle dimers are therefore an excellent platform to investigate FRET in the context of intense electric field confinement and enhancement. To assess the occurrence of FRET in the plasmonic nanoantenna, we observe a further lifetime reduction of the donor emission in the presence of the acceptor for both the 40 and 60 nm dimers (Figure 2c,d).

In the presence of the acceptor, the donor decay rate constant becomes Γ_{DA} and is higher than Γ_{Do} by the new decay rate constant Γ_{FRET} opened by the energy transfer process: $\Gamma_{DA} = \Gamma_{Do} + \Gamma_{FRET}$ (Figure 2e). The acceleration of the donor decay dynamics due to the presence of the acceptor therefore quantifies the FRET rate constant, $\Gamma_{FRET} = \Gamma_{DA} - \Gamma_{Do}$. We observe a significant increase in Γ_{FRET} in the dimer antennas as compared to the confocal DNA reference, indicating that the antenna indeed enhances the FRET rate constant (Figure 2f). For the 40 and 60 nm dimers, Γ_{FRET} is enhanced by 5- and 4.3-

DOI: 10.1021/acsphotonics.6b00148
ACS Photonics 2016, 3, 895−903

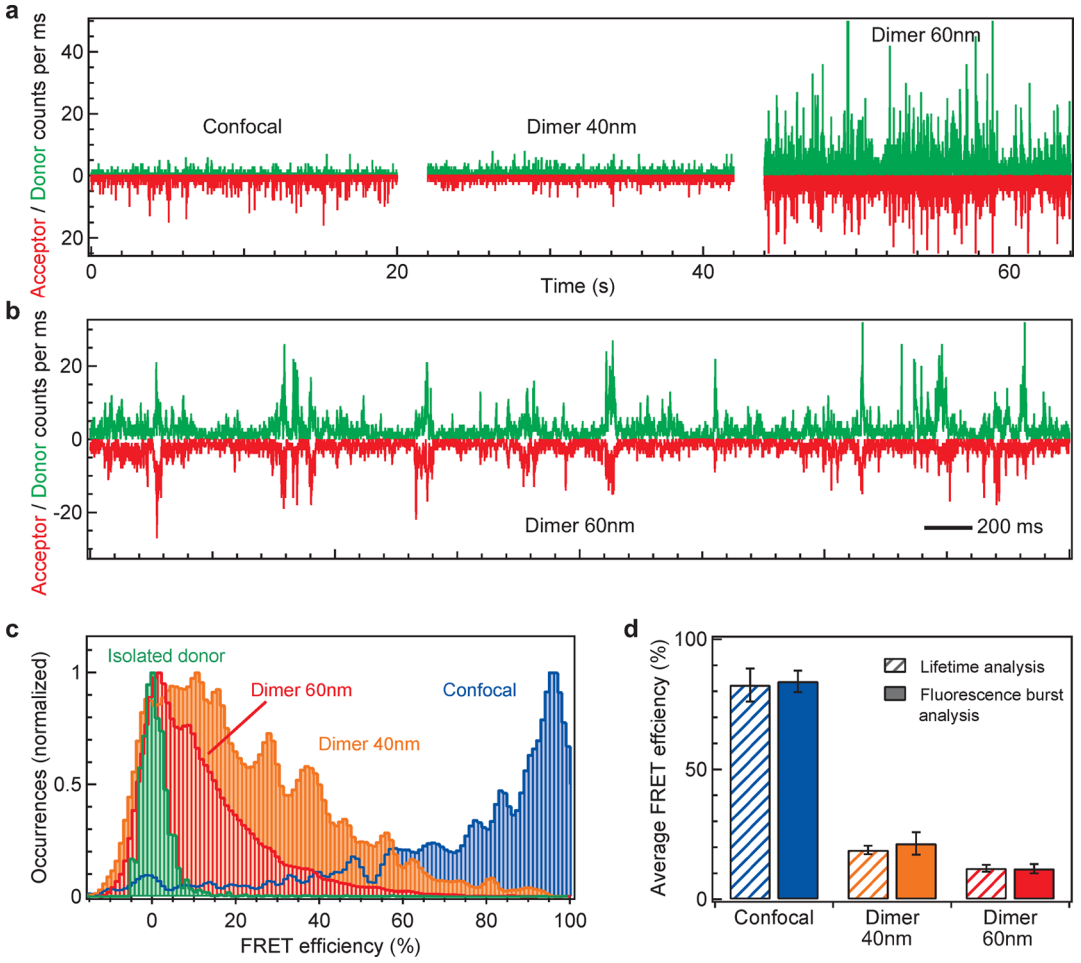

Figure 3. FRET efficiency in the gap of a gold dimer nanoantenna. (a) Fluorescence time traces for the donor (green) and acceptor (red, inverted vertical axis) detection channels for 40 and 60 nm dimers and the confocal DNA reference. The binning time is 1 ms, the total trace lasts 200 s, and the excitation power is 6.5 μW. (b) Fluorescence time traces for the 60 nm dimers as in (a) on a millisecond temporal scale to show diffusion events from individual dimers. (c) FRET efficiency histograms extracted from fluorescence burst analysis, including events with apparent negative transfer efficiency. The histogram computed for the isolated donor dye provides an independent reference for the zero FRET case (without acceptor dye). The total number of detected events is 1500 for the confocal and isolated donor, 2500 for the 40 nm dimer, and 5000 for the 60 nm dimer. (d) Comparison of average FRET efficiencies obtained from lifetime analysis (Figure 2) and the FRET histograms in (b). Both independent methods converge toward similar values.

fold, respectively. This demonstrates that a strongly confined plasmonic resonator can further accelerate nonradiative energy transfer at the nanoscale. Interestingly, this phenomenon is still observable even in the case of a short donor−acceptor separation below the classical Förster radius where the transfer rate constant without the antenna is the highest.

Next, we investigate the distributions of the fluorescence intensities for the donor and acceptor emission. Every time a FRET dimer assembly diffuses across the detection volume, it generates fluorescence bursts that are simultaneously recorded on the donor and acceptor detection channels (Figure 3a). The highest burst intensities are observed with the 60 nm dimer compared to the reference DNA case and the 40 nm dimer, in agreement with the FCS analysis of the average brightness and fluorescence enhancement per antenna construct (Supporting Information Figure S4). As compared to the FRET pairs without nanoantennas, the acceptor emission is enhanced by a factor of 2× in 60 nm dimers and quenched by a factor of 0.65 with 40 nm particles. On the other hand, the direct donor emission is enhanced by factors of 5.8 and 1.3 with 60 and 40 nm dimers, respectively (see Supporting Information Figures S5 and S6 for the fluorescence enhancement factors for the isolated donor and isolated acceptor dyes, respectively). Higher count rate enhancements for the donor dye as compared to the acceptor indicate that the overall transfer efficiency is reduced in the plasmonic antennas, while the brightness of the FRET pair is enhanced with 60 nm antennas. A larger excitation enhancement of the donor associated with a higher antenna efficiency explains why the 60 nm particles allow an overall increase of the brightness of the FRET pair while the acceptor emission obtained with 40 nm dimers is slightly quenched (see Figures S8 and S9 for theoretical calculations).

For every detected burst, the ratio of acceptor fluorescence intensity to acceptor and donor intensities defines the FRET efficiency, E_{FRET} (the probability of energy transfer over all donor transition events).[36−38] Our analysis procedure carefully takes into account the direct excitation of the acceptor by the laser light, the donor emission crosstalk into the acceptor channel, and the differences in the quantum yields and detection efficiencies for the donor and acceptor emission (see Methods section for full details). The evolution of the FRET efficiency is illustrated in the histograms of Figure 3c. In

DOI: 10.1021/acsphotonics.6b00148
ACS Photonics 2016, 3, 895−903

the absence of the plasmonic antenna, the FRET efficiency peaks at 95% for the confocal DNA reference, in agreement with the short 4 nm donor−acceptor separation as compared to the 6.5 nm Förster radius. The dispersion in FRET efficiencies is related to the fluctuations in the mutual orientations of the donor and acceptor dipoles, as already reported for similar constructs.[50−53] In the case of the gold antenna dimers, we observe a strong reduction of the FRET efficiency distribution as the donor decay rate is increased. However, the efficiencies clearly remain above zero since the distributions are significantly shifted toward larger FRET efficiencies compared to the histogram measured for the isolated donor dye (Figure 3c, green curve). This further substantiates the occurrence of FRET in the gold dimer antennas. The evolution of the FRET efficiency is further evidenced by computing the average FRET efficiency and comparing it to the value $E_{FRET} = \Gamma_{FRET}/(\Gamma_{FRET} + \Gamma_{Do}) = 1 - \Gamma_{Do}/\Gamma_{DA}$ found from the fluorescence lifetime analysis (Figure 3d). Both methods agree remarkably well, which confirms the validity of our observations.

DISCUSSION

The reduction of the FRET efficiency in the nanoantennas means that the donor decay rate Γ_{Do} increases significantly more that the FRET rate constant Γ_{FRET} in the plasmonic resonator. The dimer nanoantenna interacts efficiently with the far-field and disrupts the nonradiative FRET transfer between donor and acceptor dyes. In the hypothesis that the antenna does not influence Γ_{FRET}, the 100× lifetime reduction in the 40 nm dimer would lead to an expected 4.5% average FRET efficiency. For 60 nm dimers, the higher 150× lifetime reduction would then lead to an even lower FRET efficiency of 3.0%. However, for both nanoparticle diameters, we clearly observe FRET events with efficiencies higher than 10%, which in turn indicate that the antenna also increases the FRET rate constant. We therefore conclude that the FRET efficiency loss in the antenna is partly compensated by an enhanced FRET rate constant. To better show this enhanced FRET rate constant, we plot the distributions of the FRET rate constant following $\Gamma_{FRET} = \Gamma_{Do}E_{FRET}/(1 - E_{FRET})$, where Γ_{Do} is the isolated donor decay rate constant obtained from time-correlated lifetime measurements (Figure 4a). The box plots in Figure 4b clearly show an increase in the FRET rate constant in the dimers as compared to the reference DNA case and almost similar FRET rate constants for both dimer sizes.

Overall, we observe that the 40 nm dimers feature the highest increase of the FRET rate constant but a quenched acceptor emission, while, with 60 nm nanoparticles, the brightness of the FRET pair is enhanced but the transfer efficiency is the lowest. In practice, increasing the particle size leads to faster donor decay dynamics but not larger values of Γ_{FRET} and thus lower transfer efficiencies. These measurements also demonstrate that the count rate of the acceptor luminescence in dimers is mostly governed by the enhancement of the donor excitation and by the acceptor emission efficiency but not by the yield of the transfer process.

Numerical simulations based on Mie theory confirm the experimental observations. The distribution of the nonradiative transfer rate is estimated using classical electrodynamics by computing the power dissipated in the acceptor by the donor emission dipole.[11] The enhancement in the FRET rate constant thus evolves as the square of the electric field emitted by the donor at the position of the acceptor, projected on the axis of the acceptor transition dipole.[11,27] We thus calculate the ratio of

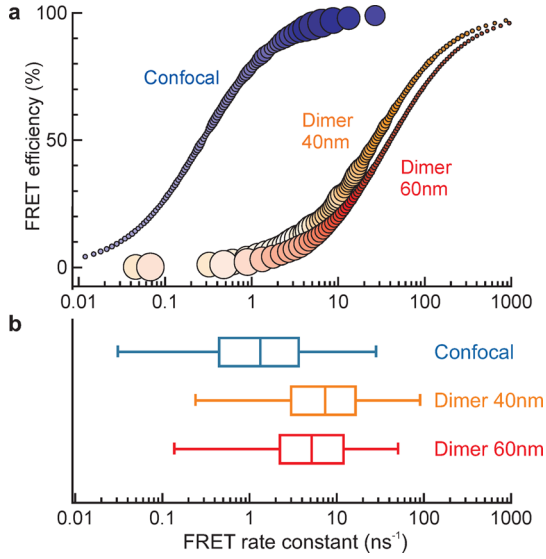

Figure 4. FRET rate constant enhancement in plasmonic dimer nanoantennas. (a) FRET efficiency as a function of the FRET rate for 40 and 60 nm dimers and the confocal DNA reference. The FRET efficiency is obtained from the fluorescence burst analysis (Figure 3); the FRET rate constant is derived following $\Gamma_{FRET} = \Gamma_{Do}E_{FRET}/(1 - E_{FRET})$, where Γ_{Do} is the isolated donor decay rate constant obtained from time-correlated lifetime measurements. The marker size is proportional to the number of occurrences found in the FRET efficiency histograms. (b) To emphasize the FRET rate constant increase in the nanoantennas, the box plots represent the first and third quartiles; the band inside the box indicates the median, and the whiskers display the second and 98th percentiles. Over 2000 detection events are considered for each case.

the field intensity distribution $|E_D(r_A)|^2$ created by the donor at the position of the acceptor, with and without the plasmonic nanoantenna. The computed spatial distributions of Γ_{FRET} enhancements are given in Figure 5 for 40 and 60 nm dimers.

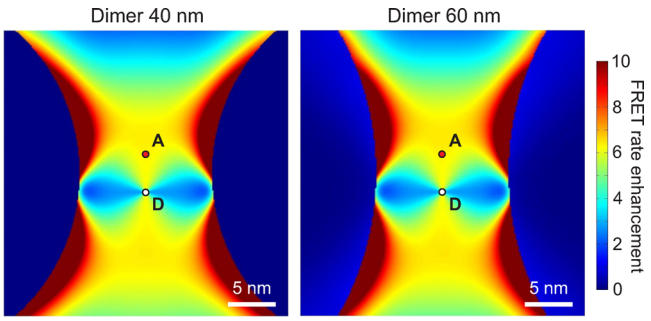

Figure 5. Mie theory calculations of the FRET rate enhancement in the 14 nm gap of 40 and 60 nm dimer nanoantennas. The position of the donor dye corresponds to the white dot D. The position of the acceptor corresponding to the experiments is indicated by the red dot A. The dark blue regions represent the gold nanoparticles.

These calculations indicate zones of enhanced energy transfer within the nanogap.[38] At the position of the acceptor molecule, we find a FRET rate constant enhancement of ∼6× for both dimer sizes, which stand in good quantitative agreement with the experimental results in Figure 2f and Figure 4b. Despite the significant LDOS difference between 40 and 60 nm dimers, Figure 5 confirms similar values found for the enhancement of the FRET rate constant.

DOI: 10.1021/acsphotonics.6b00148
ACS Photonics 2016, 3, 895−903

In the current debate about the role of the LDOS on the FRET process,[31,36−43,45] our present study demonstrates that the FRET rate can be enhanced using resonant nanogap antennas. Importantly, our experiments are carefully performed at the single-emitter level with deterministic control on the emitters' positions inside the nanogap. These results confirm the trend observed previously using nanoapertures[36,37] and planar aluminum nanoantennas[38] but with nanoscale control of the emitters' positions and highly resonant LDOS conditions. A design principle to optimize the brightness of a FRET pair with a photonic resonator would therefore feature resonances close to the donor excitation and acceptor emission wavelengths but with limited spectral overlap with the donor emission spectrum in order to leave the transfer efficiency unchanged.[14,39] Alternatively, a strong enhancement of nonradiative energy transfer rates between fluorescent dyes, without increasing significantly competitive decay channels in the donor molecule, would require a plasmonic resonator that exhibits a dark or subradiant mode[54,55] overlapping with the donor emission spectrum instead of the strongly radiating longitudinal mode of a gold nanoparticle dimer.

CONCLUSIONS

We have explored Förster resonance energy transfer between a pair of fluorescent donor and acceptor molecules deterministically placed in the nanogap of a gold nanoparticle dimer using a short DNA double strand. The resonance wavelength of the plasmonic antenna matches the donor emission spectrum, which, in combination with the intense optical confinement inside the dimer gap, leads to an enhancement of the donor decay dynamics exceeding 100-fold. Our FRET measurements, monitoring both the donor lifetime reduction and the acceptor fluorescence brightness, provide solid evidence for the acceleration of the FRET process in gold nanoparticle dimers, associated with an increase of the acceptor brightness for 60 nm particles. We obtain a 5-fold enhancement of the FRET rate constant, in good agreement with theoretical calculations, which leads to a strong reduction of the transfer efficiency when compared to competitive decay processes in the donor molecule. These results highlight the complex interaction of broadband resonators with multiple emitters, influencing both the absorption and emission of photons in the far-field, but also nonradiative coupling in the near-field.

METHODS

FRET Sample Preparation. The gold nanoparticle (AuNP) dimer assembly and purification is adapted from protocols used to produce DNA-templated plasmonic antennas featuring preferentially a single fluorescent molecule.[48,56] In brief, commercial 40 and 60 nm diameter AuNPs (BBI, UK) are coated with a negatively charged phosphine ligand (BSPP, Strem Chemicals, USA), then rinsed and concentrated by centrifugation. DNA functionalized AuNPs are obtained by incubating 120 fmol of 40 nm AuNPs (respectively 48 fmol of 60 nm AuNPs) with 0.6 pmol (respectively 2 pmol) of a 5′-trithiolated 30-base-long DNA single strand (Fidelity Systems, USA) in a 25 mM NaCl (respectively 13 mM NaCl)/1.5 mM BSPP solution with a final volume of 30 μL (respectively 40 μL). Two complementary DNA sequences are used with one featuring an ATTO550 modification in its center and the other a ATTO647N molecule. For reference samples with only one emitter, an unmodified trithiolated sequence is used with a dye-modified complementary oligo.

After an overnight incubation, the DNA-conjugated 40 nm (respectively 60 nm) particles are incubated with a $7 \times 10^5\times$ (respectively $2 \times 10^6\times$) excess of thiolated/methyl-terminated ethylene glycol hexamer (Polypure, Norway) for 30 min. The 40 nm (respectively 60 nm) samples are then purified by electrophoresis in a 1.5% weight (respectively 1%) agarose gel using a 0.5× Tris-borate EDTA running buffer. These experimental conditions are used to ensure that a large majority of recovered gold particles are not functionalized by thiolated DNA strands and that the amount of AuNPs functionalized by more than one DNA strand remains negligible. This is verified, after hybridization of the complementary sequences, by the formation of dimers and a negligible amount of larger aggregates.[48,56] In practice, the passivated DNA-functionalized 40 nm (respectively 60 nm) AuNPs are cut from the gel and concentrated by centrifugation before being incubated overnight in stoichiometric amounts in 30 mM (respectively 15 mM) NaCl. The obtained suspensions are once again purified by gel electrophoresis (1% weight), and the second fastest band, corresponding to the dimer samples, is cut and recovered from the gel (Figure S1). The 30-base-long DNA sequences are the following: 5′-trithiol-TGCTGTTCCC-ATCTXGTCCAGGTTTCGTGC-3′ (X = atto550 on G base); 5′-trithiol-GCACGAAACCTGGACXAGATGGGAACAGCA-3′ (X = atto647N on C base) The reference samples without gold nanoparticles are obtained by incubating 1 μmol of the complementary sequences (featuring a dye molecule or unmodified) in a 100 mM NaCl/10 μL solution that is heated to 80 °C and left to cool overnight.

Experimental Setup. Experiments are performed on a confocal microscope with a Zeiss C-Apochromat 63× 1.2NA water-immersion objective. The excitation source is an iChrome-TVIS laser (Toptica GmbH) delivering 3 ps pulses at 40 MHz repetition rate and 558 nm wavelength. The laser beam has a waist of 320 nm at the focal spot of the 1.2 NA objective (as determined by FCS experiments on free Alexa Fluor 647 dyes). The average excitation power is set to less than 6.5 μW to avoid entering the fluorescence saturation regime. In this excitation power, the maximum temperature increase is computed to be less than 1 °C.[57] The laser excitation is filtered by a set of two bandpass filters (Chroma ET525/70 M and Semrock FF01-550/88). Dichroic mirrors (Chroma ZT594RDC and ZT633RDC) separate the donor and acceptor fluorescence from the reflected laser light. The detection is performed by two avalanche photodiodes (Micro Photon Devices MPD-5CTC with <50 ps timing jitter) with 620 ± 20 nm (Chroma ET605/70M and ET632/60M) and 670 ± 20 nm (Semrock FF01-676/37) fluorescence bandpass filters for the donor and acceptor channels, respectively. The photodiode signal is recorded by a fast time-correlated single photon counting module (Hydraharp400, Picoquant GmbH) in time-tagged time-resolved (TTTR) mode. Each trace duration is typically 200 s. The temporal resolution for fluorescence lifetime measurements is 37 ps at half-maximum of the instrument response function.

Fluorescence Lifetime Analysis. The TCSPC histograms are fitted using Levenberg−Marquard optimization, implemented using the commercial software Symphotime 64 (Picoquant GmbH) and taking into account the reconvolution by the instrument response function. The time interval for fit is set to ensure that at least 90% of the detected count events are

DOI: 10.1021/acsphotonics.6b00148
ACS Photonics 2016, 3, 895−903

taken into account in the region of interest. The donor fluorescence decays are fitted with a three-exponential model. The short lifetime contribution is fixed to 5 ps and used to account for the noise originating from the gold photoluminescence and the Raman scattered light from the solvent. All fit results are given in the Supporting Information, Table S1. For the reference DNA sample in confocal detection, the donor emission in the FRET pair is essentially quenched, and consequently we detect a relatively larger contribution from the emission of the donor when the acceptor is not fluorescing. Therefore, the long decay term represents essentially the isolated donor, so we consider only the intermediate fluorescence decay time to quantify the FRET rate. For each sample, two sets of measurements are performed to determine the donor lifetime in the presence of the acceptor, $\tau_{DA} = 1/\Gamma_{DA}$, and the isolated donor lifetime in the absence of acceptor, $\tau_{Do} = 1/\Gamma_{Do}$. The FRET efficiency is then obtained as $E_{FRET} = 1 - \Gamma_{Do}/\Gamma_{DA} = 1 - \tau_{DA}/\tau_{Do}$, and the FRET rate constant is obtained as $\Gamma_{FRET} = \Gamma_{DA} - \Gamma_{Do}$.

FRET Efficiency Analysis. For every fluorescence burst, the number of detected photons in the acceptor channel n_a and in the donor channel n_d is recorded. The FRET efficiency is then computed according to the formula

$$E_{FRET} = \frac{n_a - \alpha n_d - n_{ao}^{de}}{n_a - \alpha n_d - n_{ao}^{de} + \gamma n_d} \quad (1)$$

This expression is more complex than the simple estimate of the FRET efficiency as the ratio $n_a/(n_a + n_d)$ of acceptor emission events over all acceptor and donor events. Several additional effects are taken into account to avoid experimental artifacts in the FRET analysis. These effects include the donor emission crosstalk into the acceptor channel, the direct excitation of the acceptor by the laser light, and the difference in the quantum yields and detection efficiencies of the donor and acceptor emission. α is the crosstalk parameter defined as the ratio of donor-only fluorescence falling into the acceptor detection channel as compared to the donor-only signal detected in the donor channel. We experimentally measure α from the intensity levels obtained with the isolated donor on both detectors. For all our measurements, we find a constant $\alpha = 0.17$ that is not noticeably affected by the dimer antenna. n_{ao}^{de} is the number of detected photons resulting from the direct excitation of the acceptor dye by the laser light. This parameter is carefully measured for every antenna by recording the average number of detected photons per burst when only the acceptor dye is present. Equation 1 also corrects for the photoluminescence from the metal for both the donor and acceptor detection channels via the terms αn_d and n_{ao}^{de}. Lastly, $\gamma = \kappa_a\phi_a/\kappa_d\phi_d$ accounts for the differences in quantum yields (ϕ_a and ϕ_d) and fluorescence detection efficiencies (κ_a and κ_d) between the acceptor and donor. For the confocal reference and the box apertures, we estimate $\gamma_{ref} = 1.3$ in the case of our setup.[36,37] For the antenna, the ratio γ is increased by the ratio of the fluorescence enhancement factors $\eta_{F,a}$ and $\eta_{F,d}$ for the isolated acceptor and isolated donor: $\gamma_{ant} = \gamma_{ref}\eta_{F,a}/\eta_{F,d}$ since both acceptor and donor dyes undergo the same excitation enhancement in the antenna. We set the ratio γ_{ant} using the values of the fluorescence enhancement factors $\eta_{F,a}$ and $\eta_{F,d}$ for the isolated acceptor and isolated donor, respectively, obtained from FCS analysis (Supporting Information Figures S5 and S6). For the 40 nm dimer, we find $\eta_{F,a} = 1.0$, $\eta_{F,d} = 0.75$, and $\gamma_{ant} = 1.7$. For the 60 nm dimer, we find $\eta_{F,a} = 5$, $\eta_{F,d} = 2.2$, and $\gamma_{ant} = 2.9$. The full trace analysis is implemented using the software Symphotime 64 (Picoquant GmbH).

Mie Theory Calculations. Scattering efficiencies were calculated with an in-house code based on the generalized Mie theory (GMT).[58] Due to intense coupling between nanoparticles in the dimer antenna, the GMT calculations require a high truncation order in the multipole expansion to ensure the convergence. Here we use multipole orders up to $N = 30$ for each scatterer. From the system total T matrix,[59] we derive analytic expressions for the electromagnetic properties of the antenna, such as decay rates, local fields, and far-field emission.[58] Single fluorescent molecules are modeled as dipolar electric sources by taking the first electric term in the outgoing multipole expansion. The total and radiative decay rate enhancements are then obtained by normalizing the emitted power in the presence of the antenna by the emitted power in the homogeneous background medium, P_0.[58,60] Notably, the total emitted power is evaluated by time averaging $P \equiv -j_{src}E_{loc}$ over one period, where E_{loc} is the electric field produced by the source current while taking into account interactions with the antenna structure. Some of the power emanating from the dipole emitter will be dissipated in the antenna, while the rest will be radiated off into the far-field, where it can be detected. The calculation of the radiated power consists of integrating the Poynting vector in the far-field limit derived from the scattered field Mie coefficients. The expressions of the total and radiated powers are analytically derived in the multipolar framework as detailed in ref 58. The refractive index of gold was tabulated according to ref 61. The enhancement of the energy transfer rate as a function of the acceptor's position is obtained by calculating the ratio of the field intensity distribution $|E_D(r_A)|^2$ created by the donor in the presence and absence of the nanoantenna. The relative increase of $|E_D(r_A)|^2$ with the nanoantenna as compared to free space directly relates to a higher rate of energy transfer to the acceptor dipole. The relative orientation between the donor and acceptor transition dipoles is set at 68°, as estimated from the average FRET efficiency of the reference sample in Figure 3c. Since the orientation of the donor in the antenna is assumed to be random, we perform the calculation with a mean angle value of 60° between the molecular transition dipole and the axis of the dimer. These angular parameters correspond only to typical values with their dispersion inducing the broad FRET efficiency histograms of Figure 3c. Computations are performed using the GMT code. The antenna parameters are set to reproduce the fabricated dimers, with a spherical nanoparticle shape of 40 or 60 nm and a 14 nm gap.

■ ASSOCIATED CONTENT

Supporting Information

The Supporting Information is available free of charge on the ACS Publications website at DOI: 10.1021/acsphotonics.6b00148.

Cryoelectron microscopy images, dark-field scattering spectrum of 40 nm dimers, fluorescence correlation spectroscopy analysis, fluorescence enhancement of isolated donor and acceptor dyes, comparison of isolated donor decay traces, table of fluorescence lifetimes, spectral dependence of decay rate constants enhancement (PDF)

DOI: 10.1021/acsphotonics.6b00148
ACS Photonics 2016, 3, 895−903

AUTHOR INFORMATION

Corresponding Author

*E-mail: jerome.wenger@Fresnel.fr.

Present Address

§ELI-NP, Horia Hulubei, National Institute for Physics and Nuclear Engineering (IFIN-HH), 077125 Bucharest-Magurele, Romania.

Notes

The authors declare no competing financial interest.

ACKNOWLEDGMENTS

The authors thank Juan de Torres and Satish B. Moparthi for stimulating discussions on FRET experiments, as well as E. Larquet and J.-M. Guigner for the cryo-EM measurements. The research leading to these results has received funding from the European Commission's Seventh Framework Programme (FP7-ICT-2011-7) under grant agreements ERC StG 278242 (ExtendFRET). Work at Institut Langevin is supported by the Laboratoire d'Excellence (LabEx) WIFI (within the French Program "Investments for the Future") under references ANR-10-LABX-24 and ANR-10-IDEX-0001-02 PSL*.

REFERENCES

(1) Förster, T. Zwischenmolekulare energiewanderung und fluoreszenz. *Ann. Phys.* **1948**, *437*, 55−75.

(2) Roy, R.; Hohng, S.; Ha, T. A practical guide to single-molecule FRET. *Nat. Methods* **2008**, *5*, 507−516.

(3) Kühlbrandt, W.; Wang, D. N. Three-dimensional structure of plant light-harvesting complex determined. *Nature* **1991**, *350*, 130−134.

(4) Hardin, B. E.; Hoke, E. T.; Armstrong, P. B.; Yum, J. H.; Comte, P.; Torres, T.; Fréchet, J. M. J.; Nazeeruddin, M. K.; Grätzel, M.; McGehee, M. D. Increased light harvesting in dye-sensitized solar cells with energy relay dyes. *Nat. Photonics* **2009**, *3*, 406−411.

(5) Baldo, M. A.; Thompson, M. E.; Forrest, S. R. High-efficiency fluorescent organic light-emitting devices using a phosphorescent sensitizer. *Nature* **2000**, *403*, 750−753.

(6) Medintz, I. L.; Clapp, A. R.; Mattoussi, H.; Goldman, E. R.; Fisher, B.; Mauro, J. M. Self-assembled nanoscale biosensors based on quantum dot FRET donors. *Nat. Mater.* **2003**, *2*, 630−638.

(7) Deniz, A. A.; Dahan, M.; Grunwell, J. R.; Ha, T.; Faulhaber, A. E.; Chemla, D. S.; Weiss, S.; Schultz, P. G. Single-pair fluorescence resonance energy transfer on freely diffusing molecules: observation of Förster distance dependence and subpopulations. *Proc. Natl. Acad. Sci. U. S. A.* **1999**, *96*, 3670−3675.

(8) Weiss, S. Measuring conformational dynamics of biomolecules by single molecule fluorescence spectroscopy. *Nat. Struct. Biol.* **2000**, *7*, 724−729.

(9) Schuler, B.; Lipman, E. A.; Eaton, W. A. Probing the free-energy surface for protein folding with single-molecule fluorescence spectroscopy. *Nature* **2002**, *419*, 743−747.

(10) Schuler, B.; Eaton, W. A. Protein folding studied by single-molecule FRET. *Curr. Opin. Struct. Biol.* **2008**, *18*, 16−26.

(11) Novotny, L.; Hecht, B. *Principles of Nano-Optics*; Cambridge University Press: Cambridge, 2006.

(12) Drexhage, K. H. Influence of a dielectric interface on fluorescence decay time. *J. Lumin.* **1970**, *1*, 693−701.

(13) Barnes, W. L. Fluorescence near interfaces: the role of photonic mode density. *J. Mod. Opt.* **1998**, *45*, 661−699.

(14) Lodahl, P.; Van Driel, A. F.; Nikolaev, I. S.; Irman, A.; Overgaag, K.; Vanmaekelbergh, D.; Vos, W. L. Controlling the dynamics of spontaneous emission from quantum dots by photonic crystals. *Nature* **2004**, *430*, 654−657.

(15) Novotny, L.; van Hulst, N. Antennas for light. *Nat. Photonics* **2011**, *5*, 83−90.

(16) Kinkhabwala, A.; Yu, Z. F.; Fan, S. H.; Avlasevich, Y.; Mullen, K.; Moerner, W. E. Large single-molecule fluorescence enhancements produced by a bowtie nanoantenna. *Nat. Photonics* **2009**, *3*, 654−657.

(17) Punj, D.; Mivelle, M.; Moparthi, S. B.; van Zanten, T. S.; Rigneault, H.; van Hulst, N. F.; García-Parajó, M. F.; Wenger, J. A plasmonic antenna-in-box platform for enhanced single-molecule analysis at micromolar concentrations. *Nat. Nanotechnol.* **2013**, *8*, 512−516.

(18) Acuna, G. P.; Möller, F. M.; Holzmeister, P.; Beater, S.; Lalkens, B.; Tinnefeld, P. Fluorescence enhancement at docking sites of DNA-directed self-assembled nanoantennas. *Science* **2012**, *338*, 506−510.

(19) Busson, M. P.; Rolly, B.; Stout, B.; Bonod, N.; Bidault, S. Accelerated single photon emission from dye molecule-driven nanoantennas assembled on DNA. *Nat. Commun.* **2012**, *3*, 962.

(20) Khatua, S.; Paulo, P. M.; Yuan, H.; Gupta, A.; Zijlstra, P.; Orrit, M. Resonant plasmonic enhancement of single-molecule fluorescence by individual gold nanorods. *ACS Nano* **2014**, *8*, 4440−4449.

(21) Akselrod, G. M.; Argyropoulos, C.; Hoang, T. B.; Ciraci, C.; Fang, C.; Huang, J.; Smith, D. R.; Mikkelsen, M. H. Probing the mechanisms of large Purcell enhancement in plasmonic nanoantennas. *Nat. Photonics* **2014**, *8*, 835−840.

(22) Punj, D.; Regmi, R.; Devilez, A.; Plauchu, R.; Moparthi, S. B.; Stout, B.; Bonod, N.; Rigneault, H.; Wenger, J. Self-assembled nanoparticle dimer antennas for plasmonic-enhanced single-molecule fluorescence detection at micromolar concentrations. *ACS Photonics* **2015**, *2*, 1099−1107.

(23) Puchkova, A.; Vietz, C.; Pibiri, E.; Wünsch, B.; Sanz Paz, M.; Acuna, G. P.; Tinnefeld, P. DNA Origami Nanoantennas with over 5000-fold Fluorescence Enhancement and Single-Molecule Detection at 25 μM. *Nano Lett.* **2015**, *15*, 8354−8359.

(24) Govorov, A. O.; Lee, J.; Kotov, N. A. Theory of plasmon-enhanced Förster energy transfer in optically excited semiconductor and metal nanoparticles. *Phys. Rev. B: Condens. Matter Mater. Phys.* **2007**, *76*, 125308.

(25) Vincent, R.; Carminati, R. Magneto-optical control of Förster energy transfer. *Phys. Rev. B: Condens. Matter Mater. Phys.* **2011**, *83*, 165426.

(26) Pustovit, V. N.; Shahbazyan, T. V. Resonance energy transfer near metal nanostructures mediated by surface plasmons. *Phys. Rev. B: Condens. Matter Mater. Phys.* **2011**, *83*, 085427.

(27) Faessler, V.; Hrelescu, C.; Lutich, A. A.; Osinkina, L.; Mayilo, S.; Jäckel, F.; Feldmann, J. Accelerating fluorescence resonance energy transfer with plasmonic nanoresonators. *Chem. Phys. Lett.* **2011**, *508*, 67−70.

(28) Gonzaga-Galeana, J. A.; Zurita-Sánchez, J. R. A revisitation of the Förster energy transfer near a metallic spherical nanoparticle:(1) Efficiency enhancement or reduction? (2) The control of the Förster radius of the unbounded medium. (3) The impact of the local density of states. *J. Chem. Phys.* **2013**, *139*, 244302.

(29) Chang, R.; Leung, P. T.; Tsai, D. P. Effects of gain medium on the plasmonic enhancement of Förster resonance energy transfer in the vicinity of a metallic particle or cavity. *Opt. Express* **2014**, *22*, 27451−27461.

(30) Marocico, C. A.; Zhang, X.; Bradley, A. L. A theoretical investigation of the influence of gold nanosphere size on the decay and energy transfer rates and efficiencies of quantum emitters. *J. Chem. Phys.* **2016**, *144*, 024108.

(31) Andrew, P.; Barnes, W. L. Förster Energy Transfer in an Optical Microcavity. *Science* **2000**, *290*, 785−788.

(32) Finlayson, C. E.; Ginger, D. S.; Greenham, N. C. Enhanced Förster energy transfer in organic/inorganic bilayer optical microcavities. *Chem. Phys. Lett.* **2001**, *338*, 83−87.

(33) Nakamura, T.; Fujii, M.; Imakita, K.; Hayashi, S. Modification of energy transfer from Si nanocrystals to Er3+ near a Au thin film. *Phys. Rev. B: Condens. Matter Mater. Phys.* **2005**, *72*, 235412.

(34) Zhang, X.; Marocico, C. A.; Lunz, M.; Gerard, V. A.; Guńko, Y. K.; Lesnyak, V.; Gaponik, N.; Susha, A. S.; Rogach, A. L.; Bradley, A. L. Wavelength, concentration, and distance dependence of nonradiative

DOI: 10.1021/acsphotonics.6b00148
ACS Photonics 2016, 3, 895−903

energy transfer to a plane of gold nanoparticles. *ACS Nano* **2011**, *6*, 9283−9290.
(35) Zhang, X.; Marocico, C. A.; Lunz, M.; Gerard, V. A.; Guńko, Y. K.; Lesnyak, V.; Gaponik, N.; Susha, A. S.; Rogach, A. L.; Bradley, A. L. Experimental and Theoretical Investigation of the Distance Dependence of Localized Surface Plasmon Coupled Förster Resonance Energy Transfer. *ACS Nano* **2014**, *8*, 1273−1283.
(36) Ghenuche, P.; de Torres, J.; Moparthi, S. B.; Grigoriev, V.; Wenger, J. Nanophotonic Enhancement of the Förster Resonance Energy Transfer Rate with Single Nanoapertures. *Nano Lett.* **2014**, *14*, 4707−4714.
(37) de Torres, J.; Ghenuche, P.; Moparthi, S. B.; Grigoriev, V.; Wenger, J. FRET Enhancement in Aluminum Zero-Mode Waveguides. *ChemPhysChem* **2015**, *16*, 782−788.
(38) Ghenuche, P.; Mivelle, M.; de Torres, J.; Moparthi, S. B.; Rigneault, H.; Van Hulst, N. F.; Garcia-Parajo, M. F.; Wenger, J. Matching Nanoantenna Field Confinement to FRET Distances Enhances Förster Energy Transfer Rates. *Nano Lett.* **2015**, *15*, 6193−6201.
(39) Blum, C.; Zijlstra, N.; Lagendijk, A.; Wubs, M.; Mosk, A. P.; Subramaniam, V.; Vos, W. L. Nanophotonic Control of the Förster Resonance Energy Transfer Efficiency. *Phys. Rev. Lett.* **2012**, *109*, 203601.
(40) Tumkur, T.; Kitur, J.; Bonner, C.; Poddubny, A.; Narimanov, E.; Noginov, M. Control of Förster energy transfer in vicinity of metallic surfaces and hyperbolic metamaterials. *Faraday Discuss.* **2015**, *178*, 395−412.
(41) Wubs, M., Vos, W. L. Förster resonance energy transfer rate and local density of optical states are uncorrelated in any dielectric nanophotonic medium. *arXiv preprint* 2015, arXiv:1507.06212.
(42) Schleifenbaum, F.; Kern, A. M.; Konrad, A.; Meixner, A. J. Dynamic control of Förster energy transfer in a photonic environment. *Phys. Chem. Chem. Phys.* **2014**, *16*, 12812−12817.
(43) Konrad, A.; Metzger, M.; Kern, A. M.; Brecht, M.; Meixner, A. J. Controlling the dynamics of Förster resonance energy transfer inside a tunable sub-wavelength Fabry-Pérot resonator. *Nanoscale* **2015**, *7*, 10204−10209.
(44) de Dood, M. J. A.; Knoester, J.; Tip, A.; Polman, A. Förster transfer and the local optical density of states in erbium-doped silica. *Phys. Rev. B: Condens. Matter Mater. Phys.* **2005**, *71*, 115102.
(45) Rabouw, F. T.; den Hartog, S. A.; Senden, T.; Meijerink, A. Photonic effects on the Förster resonance energy transfer efficiency. *Nat. Commun.* **2014**, *5*, 3610.
(46) Busson, M. P.; Rolly, B.; Stout, B.; Bonod, N.; Larquet, E.; Polman, A.; Bidault, S. Optical and topological characterization of gold nanoparticle dimers linked by a single DNA double strand. *Nano Lett.* **2011**, *11*, 5060−5065.
(47) Busson, M. P.; Rolly, B.; Stout, B.; Bonod, N.; Wenger, J.; Bidault, S. Photonic engineering of hybrid metal-organic chromophores. *Angew. Chem., Int. Ed.* **2012**, *51*, 11083−11087.
(48) Bidault, S.; Devilez, A.; Maillard, V.; Lermusiaux, L.; Guigner, J.-M.; Bonod, N.; Wenger, J. Picosecond lifetimes with high quantum yields from single-photon emitting colloidal nanostructures at room temperature. *ACS Nano* **2016**, DOI: 10.1021/acsnano.6b01729.
(49) Lermusiaux, L.; Maillard, V.; Bidault, S. Widefield spectral monitoring of nanometer distance changes in DNA-templated plasmon rulers. *ACS Nano* **2015**, *9*, 978−990.
(50) Di Fiori, N.; Meller, A. The effect of dye-dye interactions on the spatial resolution of single-molecule FRET measurements in nucleic acids. *Biophys. J.* **2010**, *98*, 2265−2272.
(51) Dolghih, E.; Roitberg, A. E.; Krause, J. L. Fluorescence resonance energy transfer in dye-labeled DNA. *J. Photochem. Photobiol., A* **2007**, *190*, 321−327.
(52) Sindbert, S.; Kalinin, S.; Nguyen, H.; Kienzler, A.; Clima, L.; Bannwarth, W.; Appel, B.; Müller, S.; Seidel, C. A. Accurate distance determination of nucleic acids via Förster resonance energy transfer: implications of dye linker length and rigidity. *J. Am. Chem. Soc.* **2011**, *133*, 2463−2480.
(53) Kupstat, A.; Ritschel, T.; Kumke, M. U. Oxazine Dye-Conjugated DNA Oligonucleotides: Förster Resonance Energy Transfer in View of Molecular Dye−DNA Interactions. *Bioconjugate Chem.* **2011**, *22*, 2546−2557.
(54) Hao, F.; Sonnefraud, Y.; Dorpe, P. V.; Maier, S. A.; Halas, N. J.; Nordlander, P. Symmetry breaking in plasmonic nanocavities: subradiant LSPR sensing and a tunable Fano resonance. *Nano Lett.* **2008**, *8*, 3983−3988.
(55) Liu, M.; Lee, T. W.; Gray, S. K.; Guyot-Sionnest, P.; Pelton, M. Excitation of dark plasmons in metal nanoparticles by a localized emitter. *Phys. Rev. Lett.* **2009**, *102*, 107401.
(56) Lermusiaux, L.; Sereda, A.; Portier, B.; Larquet, E.; Bidault, S. Reversible switching of the interparticle distance in DNA-templated gold nanoparticle dimers. *ACS Nano* **2012**, *6*, 10992−10998.
(57) Baffou, G.; Quidant, R.; Garcia de Abajo, F. J. Nanoscale control of optical heating in complex plasmonic systems. *ACS Nano* **2010**, *4*, 709−716.
(58) Stout, B.; Devilez, A.; Rolly, B.; Bonod, N. Multipole methods for nanoantennas design: applications to Yagi-Uda configurations. *J. Opt. Soc. Am. B* **2011**, *28*, 1213−1223.
(59) Stout, B.; Auger, J. C.; Devilez, A. Recursive T matrix algorithm for resonant multiple scattering: applications to localized plasmon excitations. *J. Opt. Soc. Am. A* **2008**, *25*, 2549−2557.
(60) Bharadwaj, P.; Anger, P.; Novotny, L. Nanoplasmonic enhancement of single-molecule fluorescence. *Nanotechnology* **2007**, *18*, 044017.
(61) Palik, E.; Ghosh, G. *Handbook of Optical Constants of Solids*; Academic Press: Boston, 1998.

DOI: 10.1021/acsphotonics.6b00148
ACS Photonics 2016, 3, 895−903